Sodium Hyaluronate-Induced Ocular Hypertension in Rats Damages the Direction-Selective Circuit and Inner/Outer Retinal Plexiform Layers

Agustina Noailles,[1,3] Oksana Kutsyr,[1,3] Aloma Mayordomo-Febrer,[2–4] Pedro Lax,[1,3] María López-Murcia,[2,4] Silvia M. Sanz-González,[3,5,6] María Dolores Pinazo-Durán,[3,5,6] and Nicolás Cuenca[1,3]

[1]Physiology, Genetics and Microbiology, University of Alicante, Spain
[2]Animal Medicine and Surgery, Faculty of Veterinary Medicine, Universidad CEU Cardenal Herrera, Valencia, Spain
[3]OFTARED. Spanish Net of Ophthalmic Research. Institute of health Carlos III, Madrid, Spain
[4]Mixed Research Unit for Visual Health and Veterinary Ophthalmology CEU/FISABIO, Valencia, Spain
[5]Cellular and Molecular Ophthalmo-biology Research Group, Department of Surgery, University of Valencia, Valencia, Spain
[6]Ophthalmic Research Unit "Santiago Grisolía"/FISABIO, Valencia, Spain

Correspondence: Nicolás Cuenca. Department of Physiology, Genetics and Microbiology, University of Alicante, 03690, San Vicente del Raspeig, Alicante, Spain; cuenca@ua.es.

AN, OK and AMF are joint first authors.
MDPD and NC are joint senior authors.

Received: July 30, 2021
Accepted: April 19, 2022
Published: May 3, 2022

Citation: Noailles A, Kutsyr O, Mayordomo-Febrer A, et al. Sodium hyaluronate-induced ocular hypertension in rats damages the direction-selective circuit and inner/outer retinal plexiform layers. *Invest Ophthalmol Vis Sci.* 2022;63(5):2. https://doi.org/10.1167/iovs.63.5.2

Purpose. To assess the changes in retinal morphology in a rat model of chronic glaucoma induced by ocular hypertension.

Methods. Intraocular pressure (IOP) was surgically increased through weekly injections of sodium hyaluronate (HYA) in the anterior eye chamber of the left eye of male Wistar rats, whereas the right eyes were sham operated (salt solution). During the 10-week experimental period, IOP was measured weekly with a rebound tonometer. Retinal cryosections were prepared for histological/immunohistochemical analysis and morphometry.

Results. IOP was higher in HYA-treated eyes than in sham-operated eyes along the 10-week period, which was significant from the fourth to the nineth week. Ocular hypertension in HYA-treated eyes was associated with morphologic and morphometric changes in bipolar cells, ON-OFF direction-selective ganglion cells, ON/OFF starburst amacrine cells, and inner plexiform layer sublamina.

Conclusions. Serial HYA treatment in the rat anterior eye chamber results in mild-to-moderate elevated and sustained IOP and ganglion cell death, which mimics most human open-angle glaucoma hallmarks. The reduced number of direction-selective ganglion cells and starburst amacrine cells accompanied by a deteriorated ON/OFF plexus in this glaucoma model could lend insight to the abnormalities in motion perception observed in patients with glaucoma.

Keywords: chronic glaucoma model, retina, morphology, immunohistochemistry, direction-selective ganglion cells, starburst amacrine cells

Glaucoma is a neurodegenerative disease characterized by progressive changes in optic nerve head morphology, retinal sensitivity, and visual field performance, leading to visual impairment and blindness, and is one of the leading causes of blindness in the world.[1,2] Retinal ganglion cells (RGCs), which are the neurons whose axons make up the optic nerve, undergo apoptosis throughout the course of glaucoma.[1,3] The most prevalent form of glaucoma is open-angle glaucoma, also known as primary open-angle glaucoma or chronic glaucoma (CG), and elevated intraocular pressure (IOP) and aging are considered as the major risk factors for this disease.[4] Ocular hypertension (OHT) is currently the only modifiable risk factor of the disease and is typically therapeutically managed through medical and laser-surgery interventions. Hypotensive treatments to reduce IOP are also being investigated, but they do not always prevent the irreversible course of the glaucoma neurodegeneration.[5–7]

Animal models of glaucoma have greatly increased our understanding of this disease and have been useful to assess potential therapies, as evidenced by the variety of induced glaucoma models reported in the literature.[8,9] Artificial procedures to drive sustained IOP elevation, by mimicking the anterior/posterior signs of human open-angle glaucoma, are broadly used in glaucoma research, and the majority of these influence relevant mechanical glaucoma parameters in pretrabecular, trabecular, and post-trabecular tissues.[10–15] Microbead injection,[16] laser photocoagulation of the perilimbal and episcleral veins,[17] episcleral vein injection of hypertonic saline solution,[18] intracameral injection of hyaluronan-containing viscoelastic substances,[12,19] or a simple acute optic nerve crush,[20] are some of the most recognized

Investigative Ophthalmology & Visual Science

experimentally induced models. There are also numerous inherited animal models of high IOP glaucoma.[21] One of the best-known models is the DBA/2J mouse, an age-dependent inherited model that mirrors human disease.[22] Although this model has significantly contributed to our understanding of glaucoma pathology, it is, nevertheless, limited, because some aged DBA/2J mice develop differential retinal degeneration, with one nondiseased retina and optic nerve and one retina that has undergone complete degeneration.[8] This may be due to differences in the onset of the pressure rise in both eyes. Also, the glaucomatous-type damage may not always be associated with increased IOP, and so this model should be used wisely.[23]

Traditionally, glaucoma has been considered as a disease specifically of RGCs,[24–27] although a growing number of studies support the notion that other retinal cell types may be affected in glaucoma pathology.[22,28,29] In this context, anomalies in electroretinography responses, including alterations in the a- and b-waves, scotopic threshold responses, and oscillatory potentials, have been described in both human disease and in experimental CG models,[12,22,30–35] suggesting dysfunction in different retinal cell types. However, there are scant studies analyzing the neuronal, axonal, and synaptic changes through the retinal layering in CG models.

Against this background, we aimed to evaluate the effects of sustained IOP elevation on the cytoarchitecture and layering of the rat retina in an attempt to better understand CG and glaucoma neurodegeneration pathogenesis.

Material and Methods

Animals

Animals were treated in agreement with the corresponding approved protocol by the institutional committee for animal care of the research center at the Faculty of Medicine and Odontology, University of Valencia (Spain) (code: VSC/PEA/00197 type 2). All procedures were performed in accordance with the statement of the Association for Research in Vision and Ophthalmology (ARVO) for the use of animals in ophthalmic and vision research.

The present study used seven male Wistar rats, aged 7 weeks (200 ± 40 g). Animals were housed in clear cages and were maintained under controlled conditions of humidity and temperature (22° ± 2°C) with a 12-hour light/dark cycle and were fed standard chow and water as desired. Experimental glaucoma OHT was induced in all rats by a series of intracameral injections of sodium hyaluronate (HYA), one injection per week along 10 consecutive weeks.

To avoid additional stress, rats were always gently held by the same researcher throughout the study. Before the ocular surgery, anterior eye segment biomicroscopy was performed in both eyes using a slit lamp (Kowa SL-15, Kowa Company Ltd., Tokyo, Japan), and data were recorded.

Intraocular Pressure Recording

The IOP measurements (expressed in mm Hg) were performed in both eyes of all rats by the same investigator at the same time (8:00–9:00 a.m.) to prevent circadian variations. Measurements were recorded at baseline and weekly along the 10 consecutive weeks. We used a specific tonometer designed for rodents, the TonoLab (Icare TonoLab, Helsinki, Finland) (Fig. 1A). With this rebound tonometer, the tip of the probe contacts the central cornea six times, and the final IOP reading is an average of 4 mean single readings (Fig. 1B). Only readings with high reliability were recorded (those that appeared on the monitor without a horizontal line or with a low horizontal line).

Sodium Hyaluronate Intraocular Injection

To increase and sustain the IOP levels along the study period, we established a glaucoma model described by Benozzi et al.[30] and Moreno et al.,[19] with minor modifications addressed by Mayordomo-Febrer et al.[12] Briefly, after weekly eye examination, rats were anesthetized with isoflurane (Isoflo; Laboratorios Esteve, Barcelona, Spain) and positioned under the microscope (OMS-90 operator; Topcon, Barcelona, Spain) to better visualize the anterior eye segment. Using a Hamilton syringe (Hamilton GASTIGHT Syringes, 1700 Series, Luer tip; Sigma-Aldrich Corp., St. Louis, MO, USA) with a 30-gauge needle, a temporal clear corneal paracentesis was performed with the needle bevel up through the cornea (closest to the scleral-corneal limbus) (Fig. 1C). The left eye received 25 µL of the viscoelastic substance HYA (10 mg/ml; Z-Hyalin Zeiss, Valencia, Spain), which was slowly introduced into the anterior chamber (Fig. 1C). Subsequently, Castroviejo forceps were placed on the paracentesis to avoid reflux. The right eye was sham-operated by injecting saline solution (B. Braun, Barcelona, Spain) as a vehicle instead of the HYA. After surgery, both eyes received topical antibiotics twice daily (Tobrex; Novartis Farmacéutica, Barcelona, Spain).

Retinal Immunohistochemistry

At the end of the experimental period, animals were euthanized with a lethal dose of pentobarbital (100 mg/kg, intraperitoneally) early in the morning. After marking the dorsal margin of the sclerocorneal limbus, the eyes were enucleated and fixed following a described protocol.[36] Cornea, lens, and vitreous body were removed, and the eyecups were embedded in Tissue-Tek OCT (Sakura Finetek, Zoeterwouden, The Netherlands) and processed to obtain vertical 16-µm cryostat sections along the nasal-temporal axis and through the optic nerve (Leica CM 1900 cryostat; Leica Microsystems, Wetzlar, Germany). Sections were mounted on slides (Superfrost Plus; Menzel GmbH and Co. KG, Braunschweig, Germany) and washed before the primary antibody incubation. Retinal sections were then incubated overnight with primary antibodies (Table).

The secondary antibodies were Alexa Fluor 555/488/633 anti-mouse, anti-rabbit, anti-goat, or anti-guinea pig (1:100; Molecular Probes, Eugene, OR, USA), as appropriate. In some cases, the nuclear marker TO-PRO 3 iodide (Molecular Probes) was added at a dilution of 1:1000. Finally, images were obtained under a Leica TCS SP8 confocal laser-scanning microscope (Leica Microsystems) and sections were processed in parallel using Adobe Photoshop 10 software (Adobe Systems Inc., San Jose, CA, USA).

Quantification of Retinal Ganglion and Amacrine Cells

The RGCs were identified by their immunoreactivity RBPMS stands for heart and RRM-expressed sequence or for brain-specific homeobox/POU domain protein 3a (Brn3a). The ON-OFF direction-selective RGCs (ooDSGCs) were labeled using an antibody against the cocaine- and amphetamine-

Investigative Ophthalmology & Visual Science

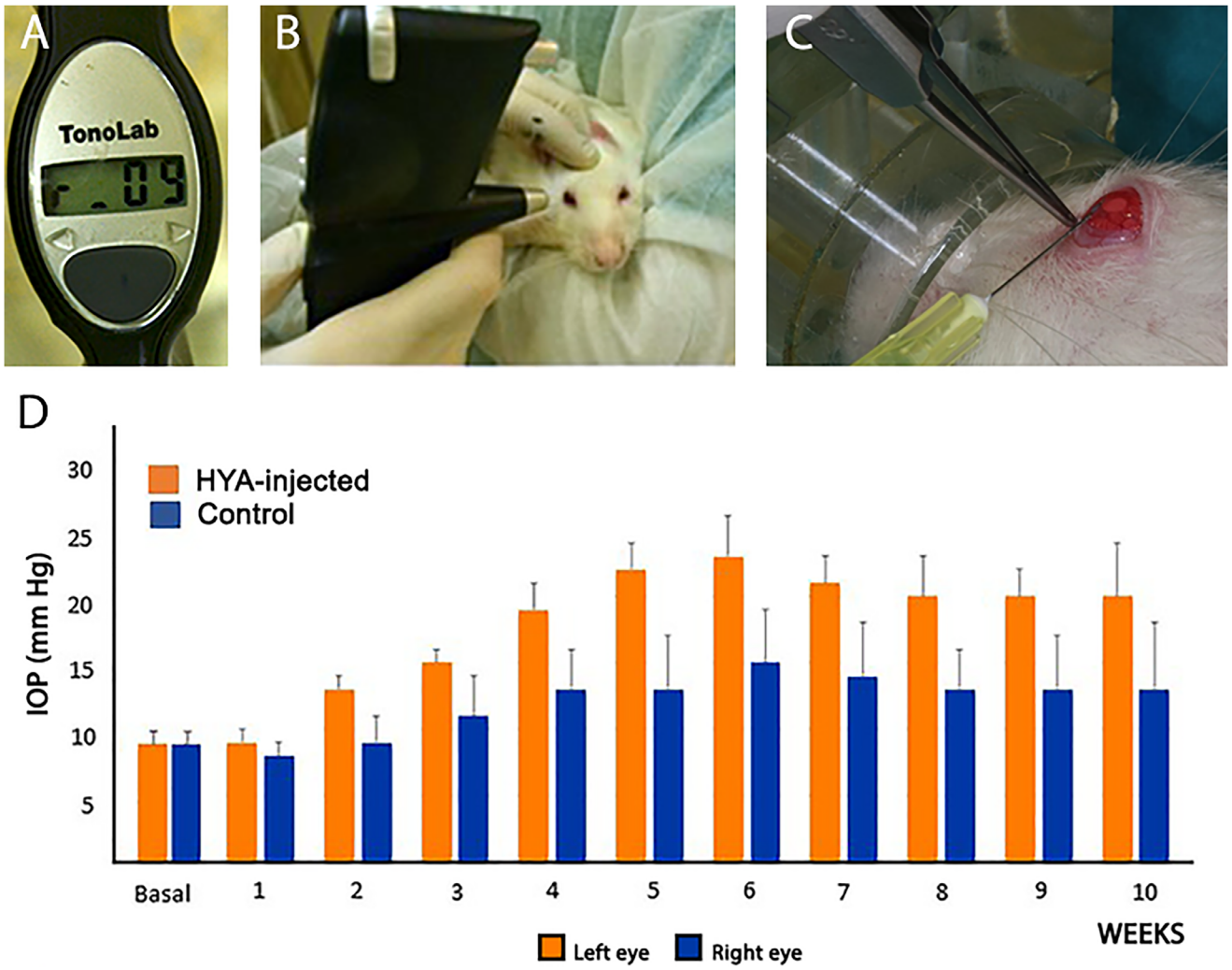

Figure 1. Animals and surgical procedures. (**A**) Tonometer TonoLab (Icare TonoLab, Finland), specific for rodents. (**B**) Measurement of IOP in the rat. (**C**) Intracameral injection of HYA in the left eye. (**D**) Evolution of IOP in the rat eyes from first week to the study end (10 weeks of injections). *Orange* indicates the left HYA-treated eye, and *blue* indicates the right control eye (sham-operated). Data are the medium ± standard deviation of six measurements per eye (n = 7 in both groups).

Table. Primary Antibodies

Molecular Marker	Source	Antibody (ref)	Dilution
Bassoon	Mouse monoclonal	*Enzo Life Sciences (ADI-VAM- PS003)*	1:1000
Calbindin D-28K	Rabbit polyclonal	*Swant (CB-38a)*	1:500
Cone arrestin	Rabbit polyclonal	*Millipore (AB15282)*	1:500
RBPMS	Rabbit polyclonal	*Provided by Dr. Brecha*	1:1000
Calretinin	Goat polyclonal	*Swant (CG1)*	1:500
α/β-PKC	Mouse monoclonal	*Santa Cruz Biotechnology (sc-80)*	1:100
Choline acetyltransferase	Goat polyclonal	*Millipore (AB144P)*	1:100
VGLUT1	Guinea Pig polyclonal	*Chemicon (AB5905)*	1:1000
Brn-3a	Mouse monoclonal	*Chemicon (MAB1585)*	1:200
CART (61-102)	Rabbit polyclonal	*Phoenix Pharma (H-003-61)*	1:200

regulated transcript (CART). Immunoreactivity to choline acetyltransferase (ChAT) was used to study starburst amacrine cells. Antibodies against calretinin and calbindin were used as markers of a large proportion of amacrine cells. To quantify positively-immunostained cells, three nonconsecutive retinal sections of the central retina from hypertensive eyes (HYA-treated) and contralateral (control) eyes (n = 7 of each) were examined. The total number of cells expressing Brn3a, CART, ChAT, calretinin or calbindin in each retinal section was determined at magnification ×63. Both groups were processed in parallel with the same confocal configuration. Data were related to the total length of the section

analyzed and then extrapolated to mm of retinal tissue using ImageJ software (NIH, Bethesda, MD, USA).

Quantification of Bipolar Cells and their Dendrites

Rod bipolar cells were identified using an antibody against the α isoform of protein kinase C (PKC). Alterations in the number and/or morphology of bipolar cells and associated dendrites were evaluated in three non-consecutive retinal sections from control and HYA-treated eyes (n = 7 of each). The total number of cells expressing PKC was determined at magnification ×63 throughout the length of every retinal section. Both groups were processed in parallel with the same confocal configuration. Data were related to the total length of the section analyzed and then extrapolated to mm of retinal tissue. Bipolar cell dendrites were assessed in four 500-μm^2 square zones at the outer plexiform layer (OPL) of each single confocal image of the central retina, close to the optic nerve. Differences in immunofluorescence signals were analyzed by obtaining the corresponding greyscale intensity (range 0–256) profile plots and quantifying the area under the intensity profile using ImageJ.

Outer Nuclear Layer Analysis and Assessment of Inner and Outer Plexiform Layer Integrity

To better characterize the changes in the retinal morphology of HYA-treated eyes, we assessed the number of photoreceptor rows and cones and the thickness of the inner nuclear layer in three nonconsecutive retinal sections of control and HYA-treated eyes (n = 7 of each). Quantification of the number of photoreceptor rows was performed in six equidistant regions (0.5, 2 and 3.5 mm from each side of the optic nerve) in the temporal-nasal axis, using TO-PRO 3 iodide. The average value for photoreceptor rows was calculated for each animal. The thickness of the inner nuclear layer was measured in four retinal regions (temporal-peripheral, temporal-central, nasal-central and nasal-peripheral). A mean value of the temporal-central and nasal-central regions was provided. The total number of cones along the temporal-nasal retinal sections was quantified using the cone arrestin antibody. Both groups were processed in parallel with the same confocal configuration. Data were related to the total length of the section analyzed and then extrapolated to mm of retinal tissue using ImageJ.

The inner plexiform layer (IPL) is divided into five distinct sublaminae of identical thickness where axons of different bipolar cells meet the dendrites of specific ganglion cells.[37–39] In the rat retina, these sublaminae can be clearly visualized by immunostaining the retina for the calcium-binding proteins calretinin and calbindin, which reveals the presence of three labeled horizontal bands of processes.[40] The external band (sublaminae 1–2) is composed of the dendrites of OFF-alpha ganglion cells, the processes of OFF-cholinergic amacrine cells, and the outer dendritic branches of direction-selective ganglion cells. This external band contains synapses and γ-aminobutyric acid type A ($GABA_A$) receptors.[41] The central band of the IPL (sublaminae 2–3) divides the OFF sublamina from the ON sublamina. Finally, the inner band of the IPL (sublaminae 3–4) includes the processes of ON-cholinergic amacrine cells, the dendrites of ON-alpha ganglion cells, the inner dendritic branches of direction-selective ganglion cells and the axon terminals of ON-bipolar cells. This inner band also contains $GABA_A$ receptors and synapses.[41]

To evaluate the synaptic connectivity and the integrity of the different sublaminae of the IPL, we calculated the fluorescence area (as described above) associated with Bassoon, calretinin, and calbindin immunostaining. Measurement of the fluorescence area was performed close to the optic nerve using ImageJ. In addition, to study the synaptic connectivity of the OPL we performed Bassoon, calbindin, and vesicular glutamate transporter 1 (VGLUT1) immunostaining. Both groups were processed in parallel with the same confocal configuration.

Statistical Analysis

Statistical analysis was done using the statistical package for the social sciences (SPSS) 26.0 software (IBM SPSS Statistics for Windows, Version IBM, Armonk, NY). A *t*-test and the Mann-Whitney U test were used to compare the mean values of the obtained parameters. One- or two-way ANOVA was used to compare the mean values of total immunoreactive cells or fluorescence area. When a 0.05 level of significance was found, post-hoc pairwise comparisons were performed using Bonferroni's test. Normal distributions and homogeneity of variance were found for the categories analyzed. *P* values <0.05 were considered to be statistically significant. Data are plotted as the mean ± SEM for retinal immunohistochemistry experiments, and mean ± SD for IOP determination.

Results

Effect of Serial Intracameral Sodium Hyaluronate Injection on Intraocular Pressure in Rats

Serial intracameral injections of HYA or vehicle along the 10-week study course induced changes in the IOP in both eyes of the rat (Fig. 1D). Control eyes (sham operated) exhibited mild, nonsignificant increases in IOP along the study, which was more evident between the fourth and seventh weeks (Fig. 1D). As expected, IOP values were significantly higher in HYA-treated eyes than in sham-operated eyes, from the fourth to the nineth week (*t*-test, $P < 0.05$, n = 7 in both groups; Fig. 1D), with a peak on the sixth week (control: 15 ± 2 mm Hg, HYA-treated: 23 ± 2 mm Hg). IOP values of HYA-treated eyes remained high and stable from the seventh to the tenth week of the study, demonstrating elevated and sustained IOP levels. Scarce iris herniation and synechia formation were detected along the experiment in either group. Also, no significant alterations in the anterior/posterior eye segment were observed in HYA-treated or control eyes.

Effect of Serial Intracameral Sodium Hyaluronate on Photoreceptor and Ganglion Cells

We evaluated the number of RGCs in both experimental groups at the end of the experimental period using immunohistochemistry with an antibody against Brn3a (Fig. 2). The number of ganglion cells per mm of retina was significantly (46%) lower in HYA-treated eyes than in control eyes (control: 30.6 ± 1.2 ganglion cells/mm, HYA-treated: 16.6 ± 1.0 ganglion cells/mm. ANOVA, Bonferroni's test, $P < 0.001$, n = 7 in both groups; Figs. 2A, 2B, 2E).

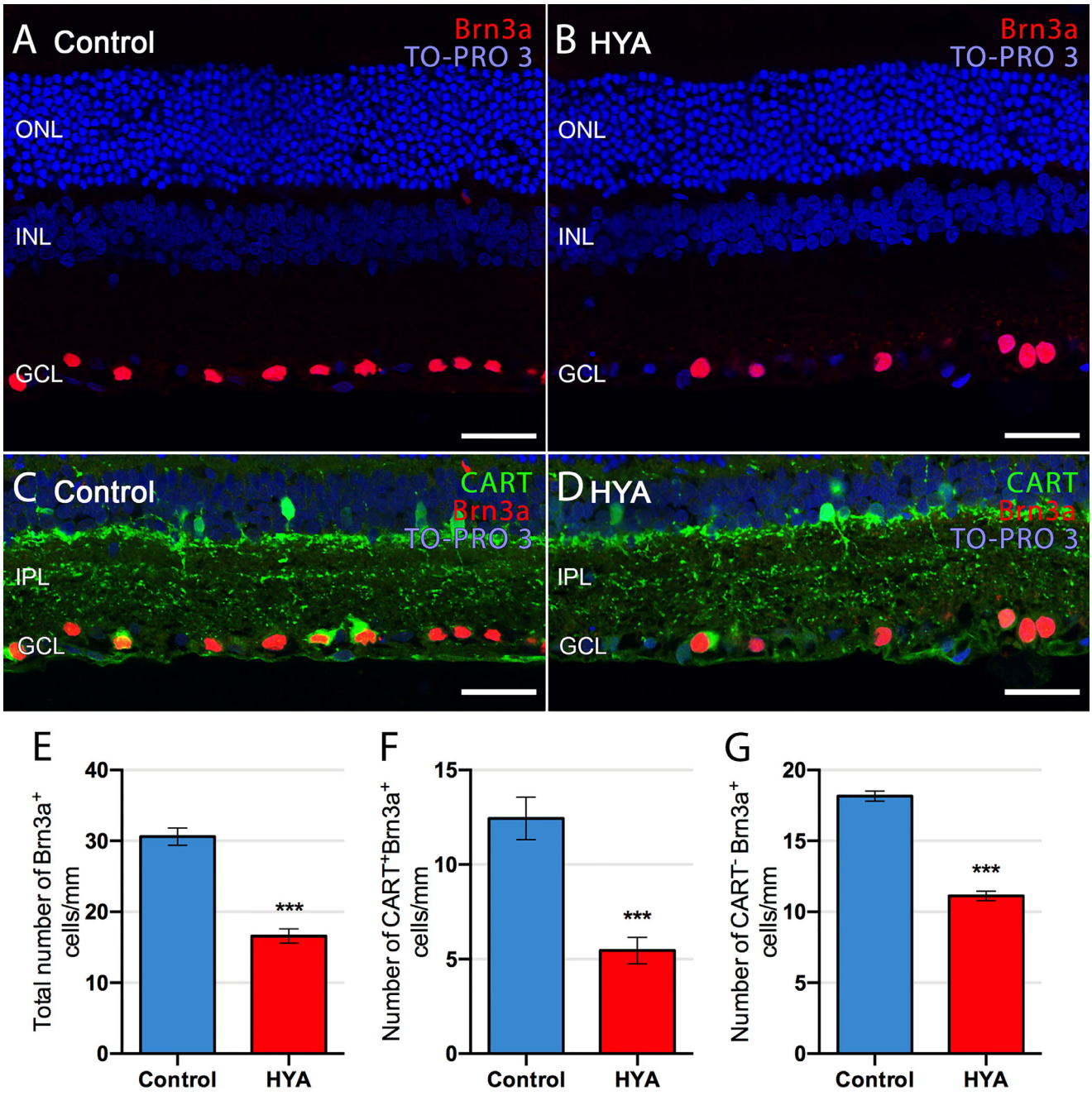

Figure 2. Quantification of ganglion cells in control and sodium hyaluronate-treated eyes. (**A–D**) Cross-sections of the central retina from control (**A, C**) and HYA-treated (**B, D**) eyes immunostained for Brn3a (**A, B**, ganglion cells; *red*) or Brn3a and CART (**C, D**, ganglion cells, *red*; ON-OFF direction-selective ganglion cells, *green*). The nuclear marker TO-PRO 3 iodide (*blue*) was used to visualize all cell nuclei. (**E–G**) Quantification of total (**E**), CART$^+$ (**F**) and CART$^-$ (**G**) ganglion cells per mm of retinal section in control (blue) and HYA-treated (*red*) eyes. ANOVA, Bonferroni's test, ***$P < 0.001$, n = 7 in each group. ONL, outer nuclear layer; GCL, ganglion cell layer. *Scale bar*: 40 µm.

We also analyzed a specific subtype of RGCs, ooDSGCs, which express the neuropeptide CART.[42,43] Immunohistochemistry analysis showed that CART labeling was poorer within the ganglion cell layer of HYA-treated eyes than of control eyes (Figs. 2C, 2D). Quantification of CART-positive RGCs (Fig. 2F) versus those lacking this marker (Fig. 2G) showed a greater loss of ooDSGCs over other RGCs in HYA-injected eyes than in control eyes. Specifically, the number of ooDSGCs per mm of retina was significantly lower (56%) in HYA-treated eyes than in control eyes (control: 12.4 ± 1.1 CART$^+$Brn3a$^+$/mm, HYA-treated: 5.5 ± 0.7 CART$^+$Brn3a$^+$/mm, ANOVA, Bonferroni's test, $P < 0.001$, n = 7 in both groups; Fig. 2F). This contrasted with the 39% reduction in the number of CART-negative RGCs per mm of retina in HYA-treated eyes relative to control eyes (control: 18.2 ± 0.4 CART$^-$Brn3a$^+$/mm, HYA-treated: 11.1 ± 0.3 CART$^-$Brn3a$^+$/mm, ANOVA, Bonferroni's test, $P < 0.001$, n = 7 in both groups; Fig. 2G). These results indicate that ooDSGCs are more susceptible than other RGCs to serial HYA-treatment.

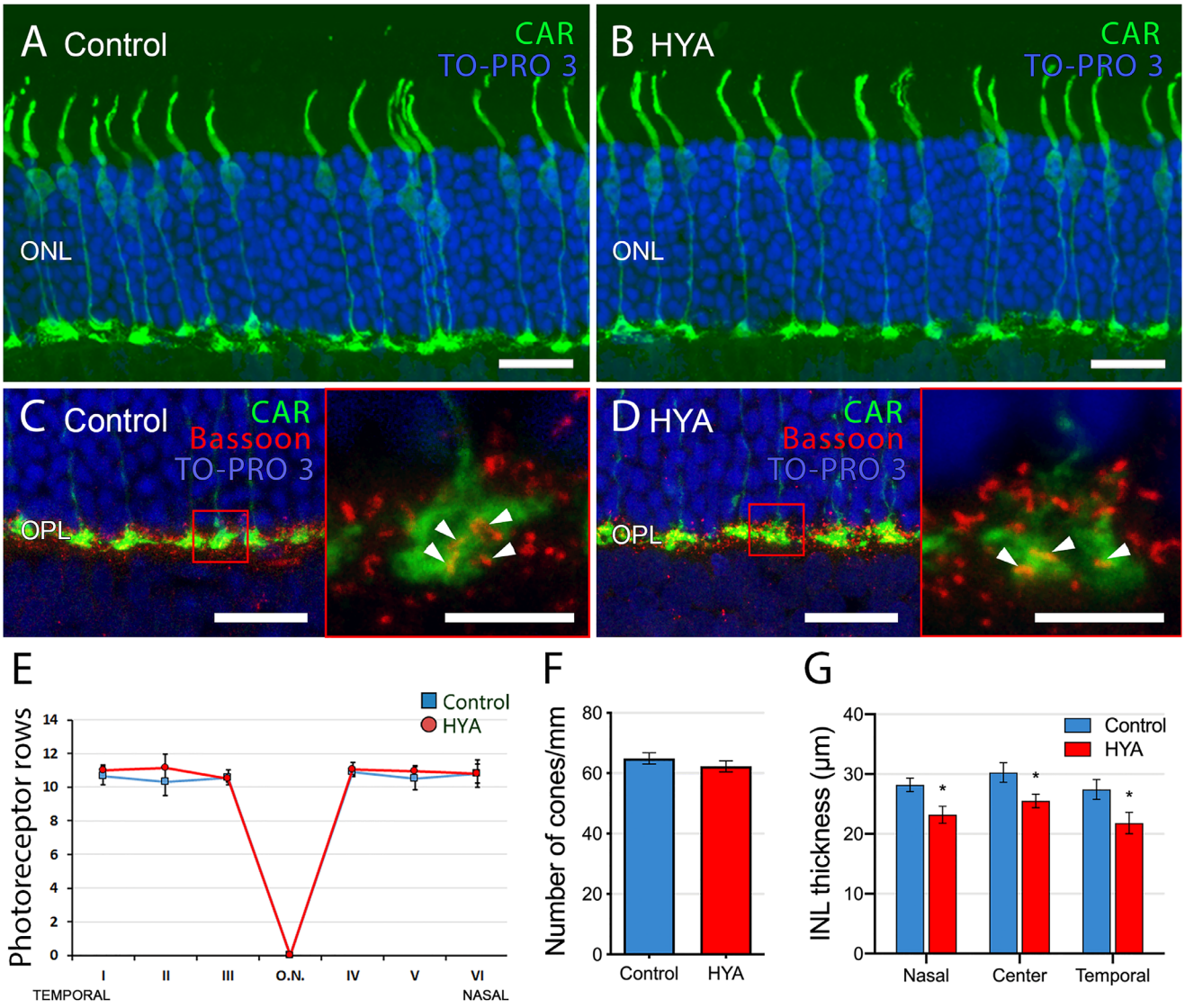

Figure 3. Number and morphology of photoreceptors in control and sodium hyaluronate-treated eyes. (**A–D**) Cross-sections of the central retina from control (**A, C**) and HYA-treated (**B, D**) eyes immunostained for cone arrestin (**A, B**, cone photoreceptors, *green*) or cone arrestin and Bassoon (**C, D**, cone photoreceptors, *green*; synaptic ribbon, *red*). The nuclear marker TO-PRO 3 iodide (*blue*) was used to visualize all cell nuclei. **Insets** show a magnification of cone pedicles and synaptic ribbons (**C, D**). *Arrowheads* point to synaptic ribbons inside cone pedicles. (**E-G**) Quantification of photoreceptor rows in ONL (**E**), cones per millimeter of retinal section (**F**) and INL thickness (**G**) in both control and HYA-treated eyes. ANOVA, Bonferroni's test, $^*P < 0.05$, n = 7 in each group. ONL, outer nuclear layer; ON, optic nerve. *Scale bar*: 20 µm (**A–D**), 5 µm (**C, D** insets).

Analysis of the cone structure in retinal sections of control and HYA-treated eyes stained with the cone arrestin antibody revealed no evident differences in cell morphology. Cone photoreceptors in control and HYA-treated eyes had a normal physiological shape with no changes in their inner and outer segments (Figs. 3A, 3B).

Analysis of TO-PRO 3 iodide-stained (nuclear) retinal sections revealed no difference in photoreceptor cell density in the two groups. Retinas of control eyes had an average of 10.6 ± 0.2 rows of photoreceptors, whereas HYA-treated eyes showed an average of 10.9 ± 0.2 photoreceptor rows (n = 7 in both groups; Fig. 3E). Likewise, retinal cone density was similar between groups (control: 64.9 ± 1.9 cones/mm, HYA-treated: 62.2 ± 1.8 cones/mm, n = 7 in both groups; Fig. 3F). By contrast, we found that inner nuclear layer (INL) thickness throughout the retinal sections was significantly lower in HYA-treated eyes than in control eyes (Fig. 3G); retinas of the control group showed an average INL thickness of 28.6 ± 0.9 µm, whereas HYA-injected eyes had an average thickness of 23.5 ± 0.9 µm (ANOVA, Bonferroni's test, $P < 0.05$, n = 7 in both groups).

Effects of Serial Intracameral Sodium Hyaluronate on Bipolar Cells and Synaptic Complexes

Our results thus far show that HYA treatment does not affect the number of photoreceptors or their morphology. However, as significant changes were found in the INL thickness, we considered that some neurons postsynaptic to photoreceptors, such as bipolar cells, could be affected by

HYA. In the rat retina, dendritic terminals of ON-rod bipolar cells make connections with rod spherules through a huge dendritic arbor in the OPL, and their axons spread into the IPL where each ends in a rounded axon terminal in the S5 stratum (Figs. 4A, 4B). Quantification of PKC-immunoreactive rod bipolar cells revealed no differences between control and HYA-treated eyes (control: 3156 ± 200 bipolar cells/mm, HYA-treated: 2968 ± 215 bipolar cells/mm, *t*-test, $P = 0.5341$, n = 7 in both groups). Nevertheless, analysis of the mean fluorescence area in the OPL revealed significant differences between experimental groups: the density of bipolar cell dendrites was significantly lower in HYA-treated eyes than in control eyes, with a mean fluorescence value of 2394.4 ± 111.6 arbitrary units (A.U.) in control eyes and 2257.7 ± 81.7 A.U. in HYA-treated eyes (ANOVA, Bonferroni's test, $P < 0.05$, n = 7 in both groups; Fig. 4I).

Based on the lower density of bipolar cell dendrites in the OPL of HYA-treated eyes, we assumed that the synaptic connectivity between photoreceptors and second-order neurons might be altered. To test this hypothesis, we used an antibody against Bassoon, a protein element of the synaptic ribbons present in rod spherules and cone pedicles. We observed an evident decrease in Bassoon expression between experimental groups (Figs. 4E, 4F). To quantify the differential expression of Bassoon, we used profile plots of mean grey intensity in each horizontal line of images exhibiting Bassoon immunofluorescence (Figs. 4G, 4H). Results showed that mean fluorescence area of the profile plots found at the OPL and IPL level was significantly lower in HYA-treated eyes than in control eyes (OPL: 496.6 ± 35.5 A.U. [control] vs. 347.4 ± 17.1 A.U. (HYA-treated); and IPL: 4091.4 ± 135.5 A.U. (control) vs 3191.9 ± 232.1 A.U. (HYA-treated); ANOVA, Bonferroni's test, $p < 0.001$ in both cases, n = 7; Figs. 4J, 4K). To explore whether the loss of synaptic ribbons at the OPL is associated with the cone pathway, we double-immunolabeled the retinas of control and HYA-treated eyes with cone arrestin and Bassoon. As illustrated in Figures 3C and 3D, cone pedicles of the retinas of both experimental groups showed a similar number of Bassoon punctae (Figs. 3C, 3D, insets). Therefore the loss of Bassoon at the OPL does not seem to be associated with alterations in the cone pathway.

To better characterize the morphology of the photoreceptor axon terminal and their contacts with secondary neurons, we used antibodies to two specific markers: calbindin (horizontal cell dendrites) and VGLUT1 (rod spherules and cone pedicles) (Figs. 5A, 5B). We could clearly discern VGLUT1 immunoreactivity in rod spherules in control eyes, and the horizontal cell endings in the synaptic triad (Fig. 5C, arrowheads). By contrast, VGLUT1 immunoreactivity was reduced in some of the photoreceptor axon terminals in HYA-treated eyes (Fig. 5D, arrowheads).

Effect of Serial Intracameral Sodium Hyaluronate on the Density of Starburst Amacrine Cells

We next assessed the number and morphology of ON/OFF starburst amacrine cells in control and HYA-treated eyes using an anti-ChAT antibody (Fig. 6). ChAT immunostaining showed that the ON/OFF plexus appeared deteriorated in HYA-treated eyes (Figs. 6A–F), with numerous gap zones (Fig. 6F, arrowheads). Moreover, we found that the total number of starburst amacrine cells was significantly lower in HYA-treated eyes than in control eyes (control: 24.8 ± 3.1 cells/mm, HYA-treated: 17.7 ± 2.9 cells/mm, ANOVA, Bonferroni's test, $P < 0.01$, Fig. 6G). Analyzing separately the OFF and ON starburst amacrine cells, we observed a significantly lower number of both in HYA-treated eyes than in control eyes (control: 13.4 ± 1.9 OFF cells/mm, 11.4 ± 1.8 ON cells/mm, HYA-treated: 9.9 ± 2.2 OFF cells/mm, 7.8 ± 1.4 ON cells/mm, ANOVA, Bonferroni's test, $P < 0.05$ OFF cells, $P < 0.01$ ON cells, n = 7 in all cases; Fig. 6G). Thus, similar to ooDSGCs, starburst amacrine cells were also highly susceptibility to serial HYA-treatment.

Effect of Serial Intracameral Sodium Hyaluronate on the Structure and Organization of the IPL Sublaminae

We next studied the structure and organization of the IPL sublaminae using two different immunostainings: calretinin and calbindin. Calretinin immunostaining revealed a clear loss of structure of the IPL sublaminae S1, S2, and S3 in HYA-treated eyes (Figs. 7A, 7B). We quantified the mean fluorescence area of the IPL sublaminae using the same method described as for Bassoon (Figs. 7C, 7D). The lower fluorescence area found in HYA-treated eyes compared with control eyes (control: 3247.6 ± 188.1 A.U., HYA-treated: 2167.6 ± 158.3 A.U., ANOVA, Bonferroni's test, $P < 0.001$, n = 7 in both groups; Fig. 7E) supports our observations on the loss of the IPL structure (sublaminae S1, S2, and S3). To establish whether the loss of IPL structure is associated with a reduction in calretinin-positive cells or a loss of processes in these cells, we quantified the number of calretinin-labeled cells in the retinas of both experimental groups. Results showed that the number of calretinin-positive cells per mm of retina was significantly lower in HYA-treated retinas than in control retinas (control: 76.3 ± 1.6 cells/mm, HYA-treated: 59.6 ± 1.6 cells/mm. ANOVA, Bonferroni's test, $P < 0.001$, n = 7 in both groups; Fig. 7F). We repeated this analysis for calbindin immunoreactivity, which confirmed the loss of labeled elements in the IPL sublaminae of HYA-treated eyes (Figs. 8A–D) (control: 2622.3 ± 424.6 A.U., HYA-treated: 1557.8 ± 360 A.U., ANOVA, Bonferroni's test, $P < 0.01$, n = 7 in both groups; Fig. 8E). Likewise, the lower fluorescence was also associated with fewer calbindin-positive cells per mm of retina in HYA-treated eyes in comparison with control eyes (control: 80.4 ± 2.1 cells/mm, HYA-treated: 54.3 ± 5.8 cells/mm. ANOVA, Bonferroni's test, $P < 0.01$, n = 7 in both groups; Fig. 8F).

Discussion

Here we used a rat model of experimental glaucoma (OHT) established by Benozzi et al.,[30] which is generated through multiple intracameral injections of HYA to increase IOP by steadily reducing the drainage of the aqueous humor. Despite the limitations of this method imposed by the repeated injections, which can be associated with several complications (cataracts, corneal edema or infections), chronic HYA injection induces significant functional and histological changes.[12,19,30,44–47] In addition to the increased and sustained IOP, significantly decreased scotopic a- and b-waves, scotopic threshold responses and oscillatory potentials have been reported in this model.[12,19,30] These functional changes point to alterations in photoreceptors and in bipolar, amacrine and ganglion cells. However, only RGC death and metabolomic profile changes have been described

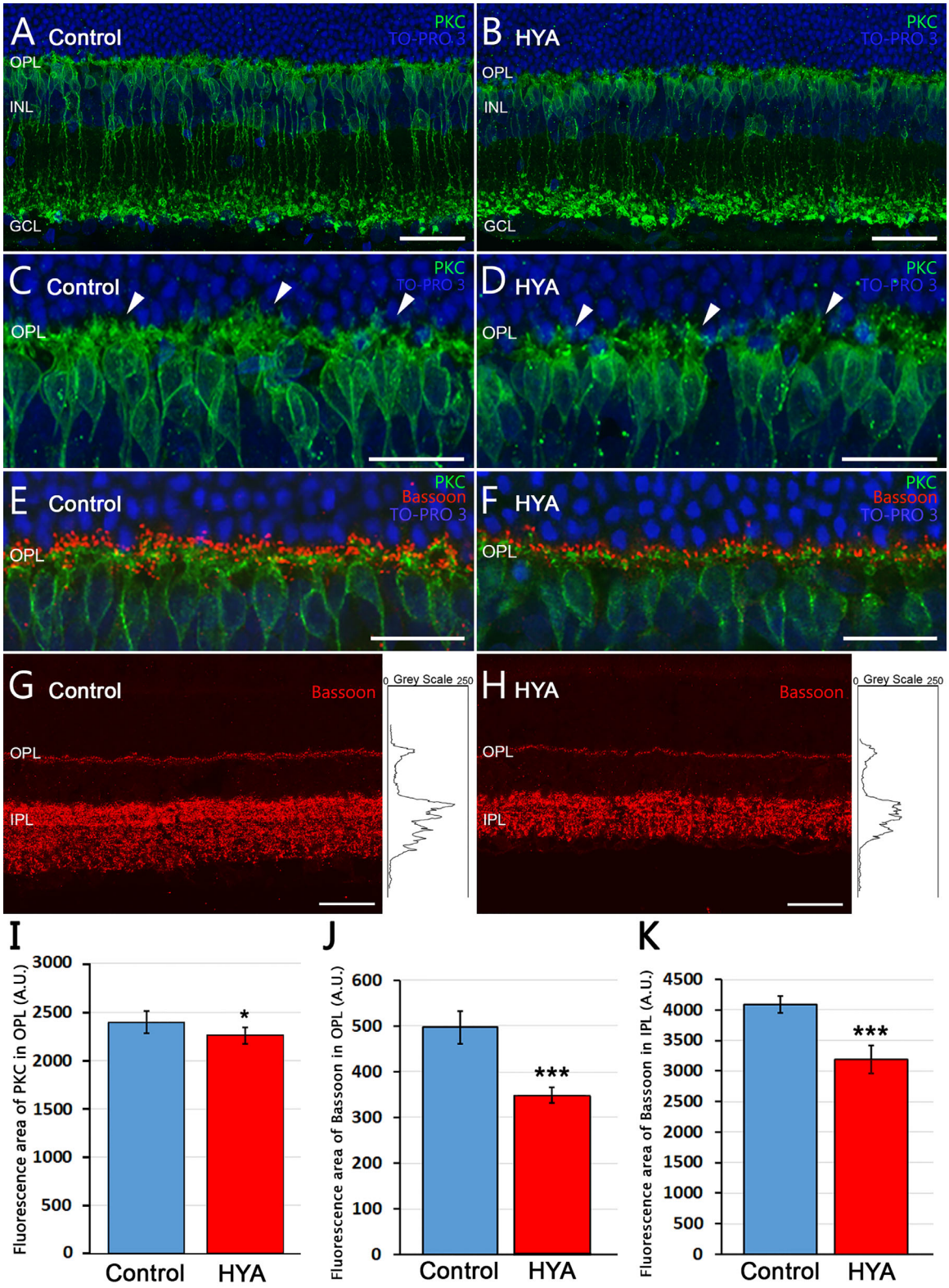

Figure 4. Bipolar cell morphology and Bassoon expression in control and sodium hyaluronate-treated eyes. (**A–F**) Cross-sections of the central retina from control (**A, C, E**) and HYA-treated (**B, D, F**) eyes immunostained for PKC (**A–D**, rod bipolar cells, *green*) or PKC and Bassoon (**E, F**, rod bipolar cells, *green*; Bassoon, *red*). The nuclear marker TO-PRO 3 iodide (*blue*) was used to visualize all cell nuclei. (**C, D**) Magnification of (**A, B**) showing the morphology of bipolar cell dendrites in control (**C**) and HYA-treated (**D**) eyes; *arrowheads* point to bipolar cells dendrites in both groups. (**E, F**) Retinal sections of control (**E**) and HYA-treated (**F**) eyes labeled with antibodies against PKC and Bassoon. (**G, H**) Representative retinal sections showing synaptic ribbons immunostained with anti-Bassoon antibodies (*red*) from control (**G**) and HYA-treated (**H**) eyes. **Right insets** show the profile plots of mean gray intensity for each horizontal line of images of the retina showing Bassoon immunofluorescence. (**I**) Quantification of PKC mean fluorescence area in the OPL of control and HYA-treated eyes. ANOVA, Bonferroni's test, n = 7 in each group, $^*P < 0.05$. (**J, K**) Quantification of Bassoon differential expression in the outer (**J**) and the

inner (**K**) plexiform layers of control (*blue*) and HYA-treated (*red*) eyes. Data are represented as mean values of fluorescence of Bassoon in areas close to the optic nerve. ANOVA, Bonferroni's test, ***$P < 0.001$, n = 7 in each group. OPL, outer plexiform layer; GCL, ganglion cell layer. *Scale bar*: 40 µm (**A, B, G, H**), 20 µm (**C–F**).

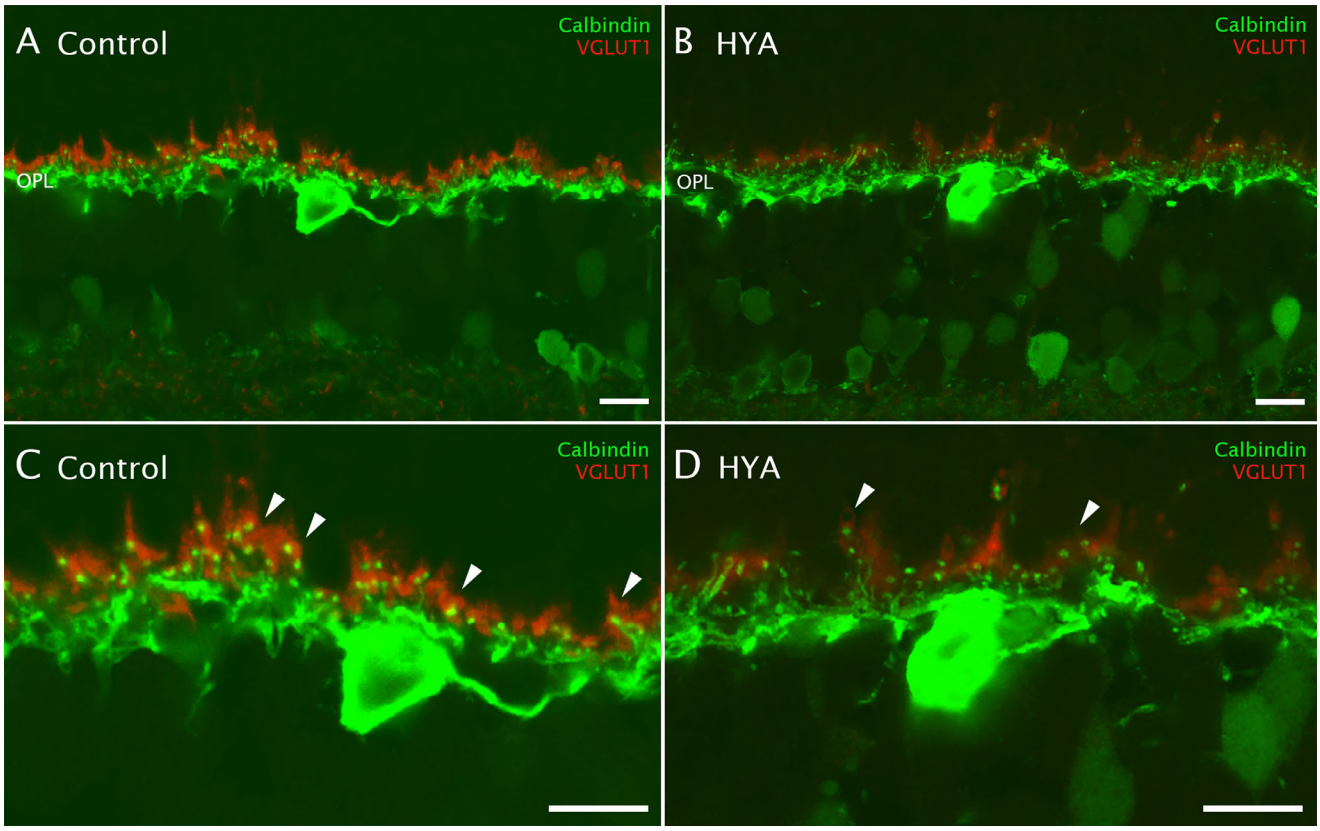

Figure 5. Effect of sodium hyaluronate on synaptic structure. (**A–D**) Cross-sections of the central retina from control (**A, C**) and HYA-treated (**B, D**) eyes immunostained with antibodies against calbindin (horizontal cell dendrites, *green*) and VGLUT1 (vesicular glutamate transporter type 1, *red*). (**C, D**) Magnification of (**A, B**) showing details of the synaptic complexes between horizontal and photoreceptor cells: some of the synaptic complexes of HYA-treated eyes exhibited lower VGLUT1 immunoreactivity (*arrowheads*) as compared with control eyes. OPL, outer plexiform layer. *Scale bar*: 10 µm (**A–D**).

so far,[12,19,30] and histological studies are needed to evaluate all possible retinal alterations in this experimental OHT/CG model.

In the present study, serial intracameral HYA-injection into the rat eye induced chronic OHT that reflected structural abnormalities evidenced by histologic and immunohistochemical analysis. Comparison of OHT-induced and contralateral rat eyes demonstrated sustained and elevated IOP that mimics most hallmarks of human CG. The high-density HYA acted mechanically by hindering the drainage of aqueous humor at the angle of the anterior eye chamber. HYA-injected eyes showed mild-to-moderate IOP increases from baseline and throughout the study, as reported previously.[12,19,30,48]

Immunostaining analysis showed that, in addition to the well-characterized loss of RGCs,[29,37,49,50] both the inner and outer retina is impaired in this glaucoma model. Sustained OHT resulted in a significant reduction in INL thickness and bipolar cell dendrites in the OPL, diminished immunoreactivity to Bassoon in the OPL and IPL, and reduced expression of VGLUT1 in the OPL, which is similar to other experimental laser-induced[51] and microbead-injected[31,43] glaucoma models, and is also seen in inherited glaucoma animals like the DBA/2J mouse.[22] Additionally, the present study shows, for the first time to our knowledge in a model of high IOP glaucoma, the loss of ON/OFF starburst amacrine cells and ooDSGCs and their plexuses at the IPL, suggesting an alteration of the direction-selective circuit.

Our results highlight structural impairment of the IPL sublaminae in HYA-treated eyes, possibly due to the alteration of retinal circuits mediated by IOP. Interestingly, in DBA/2J mice, the stratification patterns in the two synaptic layers of the retina (the OPL and IPL) do not differ when compared with control mice.[52] Previous studies in Piccolo/Bassoon knockout mice revealed that the composition of the presynaptic terminal was not significantly altered and, noticeably, abrogating the expression of the two components from synapses did not seem to alter the basic parameters of synaptic transmission.[53] Accordingly, we did not expect the loss of Bassoon expression in the IPL and OPL to be the major cause of the lower electroretinogram response observed in this animal model,[12] but it is a remarkable consequence of the increased IOP. Nevertheless, synapses are an obvious point of vulnerability in glaucoma-

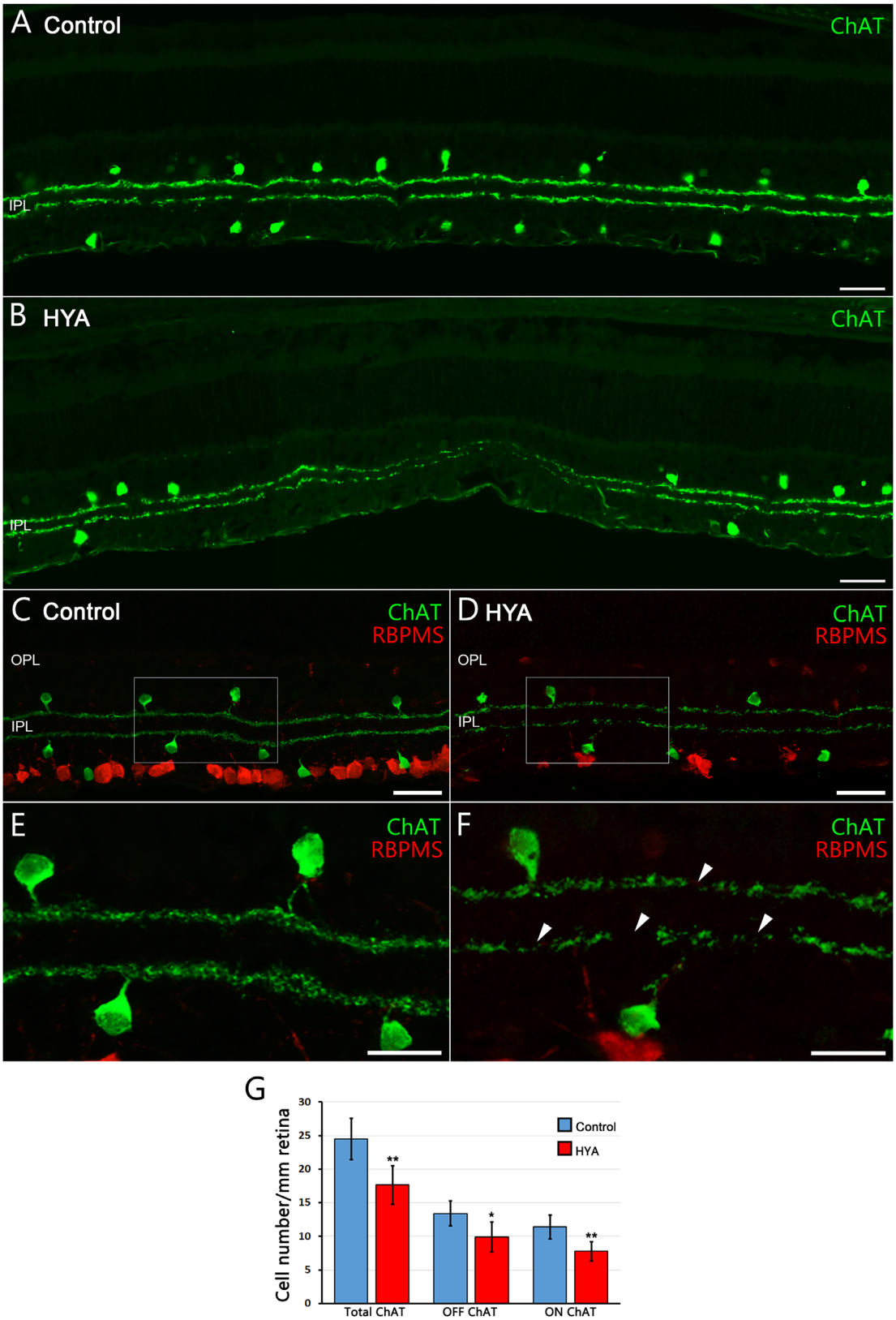

Figure 6. Starburst amacrine cells morphology and quantification in control and sodium hyaluronate-treated eyes. (**A, B**) General view of the starburst amacrine cell plexus in cross-sections of the central retina of control (**A**) and HYA-treated (**B**) eyes immunostained for ChAT (starburst amacrine cells; *green*). (**C, D**) Retinal sections of control (**C**) and HYA-treated (**D**) eyes immunostained for ChAT (starburst amacrine cells; *green*) and RBPMS (ganglion cells; red). (**E, F**) Magnification (**C, D**) shows the morphology of starburst amacrine cells and their ON/OFF plexus; *arrowheads* point to gap zones of the starburst amacrine cell plexus in HYA-treated eyes. (**G**) Quantification of total OFF and ON starburst amacrine cells per mm of retinal section in control (*blue*) and HYA-treated (*red*) eyes. ANOVA, Bonferroni's test, $^{*}P < 0.05$, $^{**}P < 0.01$, n = 7 in each group. RBPMS, heart and RRM-expressed sequence. *Scale bar*: 40 µm (**A–D**), 20 µm (**E, F**).

Investigative Ophthalmology & Visual Science

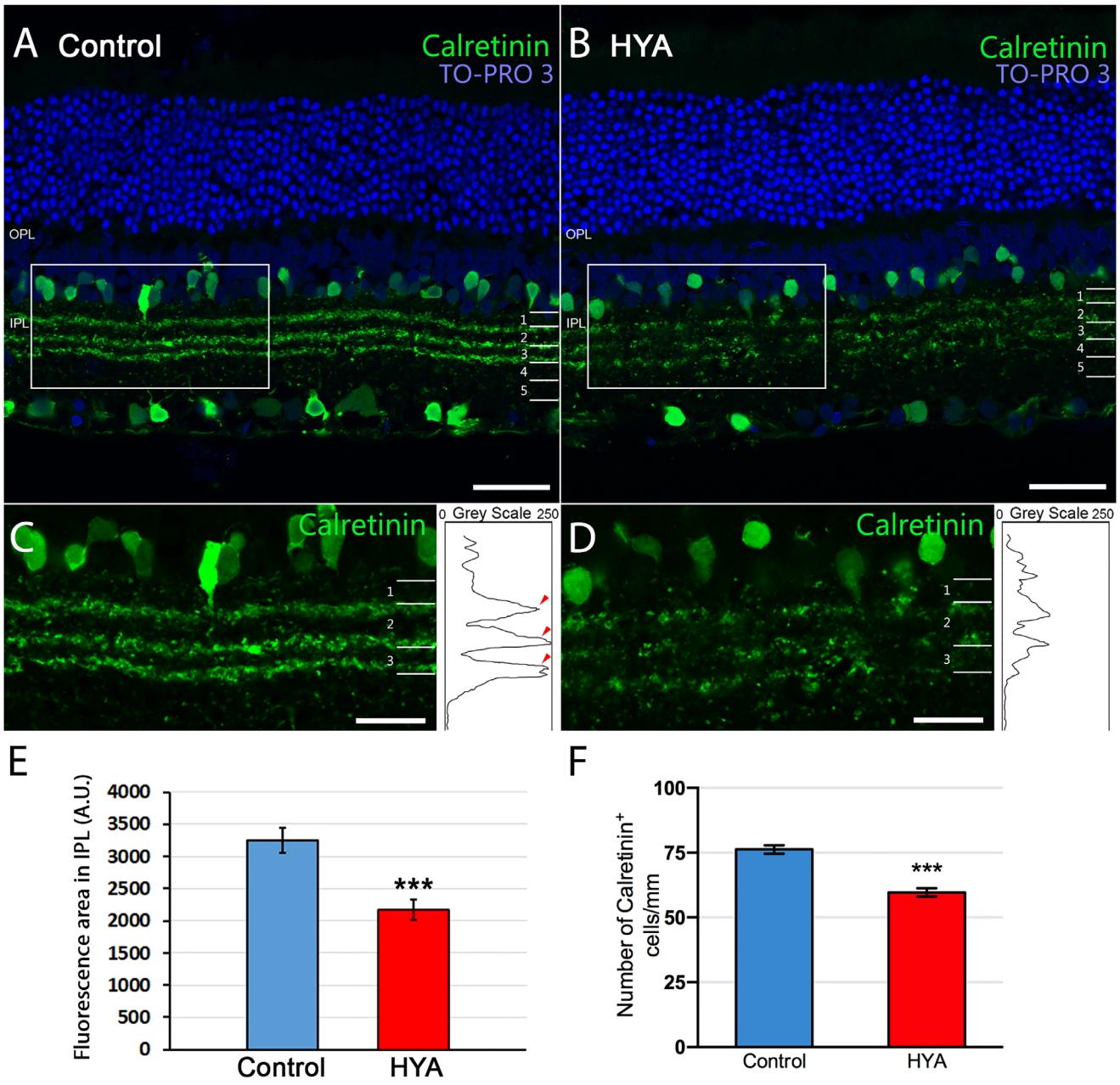

Figure 7. Characterization of the inner plexiform layer sublaminae immunostained for calretinin. (**A, B**) Cross-sections of the central retina from control (**A**) and HYA-treated (**B**) eyes stained against calretinin (some amacrine and ganglion cells, and IPL sublaminase, *green*). The nuclear marker TO-PRO 3 iodide (*blue*) was used to visualize all cell nuclei. (**C, D**) Magnification (**A, B**) shows details of IPL sublaminae. **Right insets** show the profile plots of mean gray intensity for each horizontal line of images of the retina showing calretinin immunofluorescence. (**E, F**) Quantification of calretinin expression in the IPL sublaminae (**E**) and the number of calretinin+ cells per mm of retina (**F**) of control (*blue*) and HYA-treated (*red*) eyes. Data are represented as mean values of fluorescence in areas close to the optic nerve. ANOVA, Bonferroni's test, $^{***}P < 0.001$, n = 7 in each group. *Scale bar*: 40 µm (**A, B**), 20 µm (**C, D**).

tous disease because of their energy demands and complexity.[54,55] This is evident in DBA/2J mice, in which the width of the synaptic OPL is reduced and the rod photoreceptor ribbon structure is altered,[52] as in other animal models with increased IOP.[31,56] Additionally, some studies in humans describe a loss of neurons in both outer and inner nuclear layers, which could also lead to poorer synaptic connections in the OPL.[28,57–59]

The direction-selective circuit in the retina processes the directional information of visual motion. This circuit is composed of bipolar cell subtypes, starburst amacrine cells, and ooDSGCs, which together respond to increases (ON cells) or decreases (OFF cells) in illumination.[50,60–62] Starburst amacrine cells represent a well-defined neural population that is clearly identified as the only cholinergic neurons in the retinal tissue.[63,64] This cell type is heavily overlying in distribution and is distinguished by radially symmetric dendritic trees. In the vertebrate retina, these cells are organized as mirror-symmetric pairs at both sides of the IPL. One of the mirror pairs has its cell body displaced

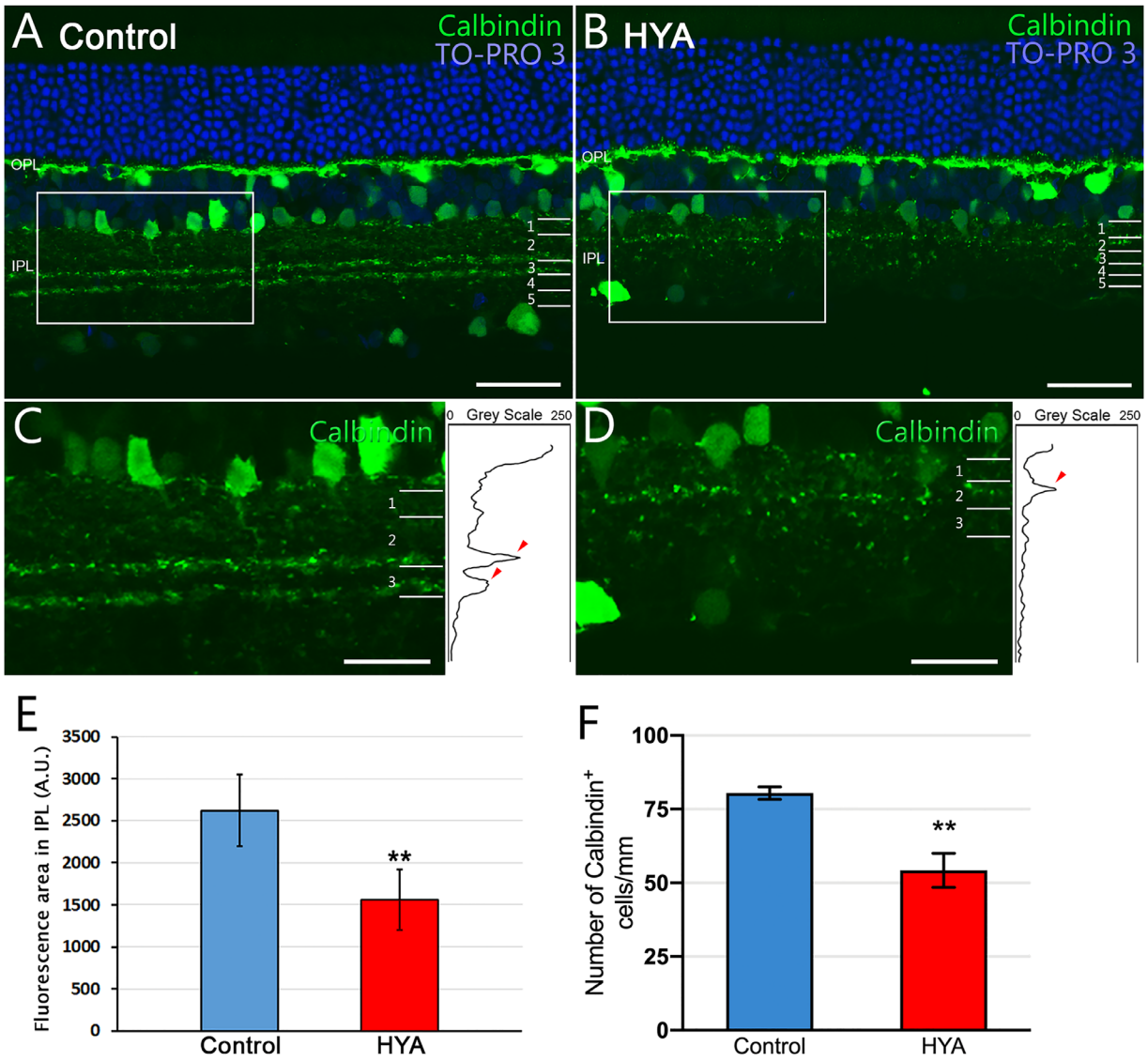

Figure 8. Characterization of the inner plexiform layer sublaminae immunostained for calbindin. (**A, B**) Cross-sections of the central retina from control (**A**) and HYA-treated (**B**) eyes immunostained for calbindin (horizontal, some amacrine and ganglion cells, and IPL sublaminae; *green*). The nuclear marker TO-PRO 3 iodide (*blue*) was used to visualize all cell nuclei. (**C, D**) Magnification (**A, B**) shows details of IPL sublaminae. **Right insets** show the profile plots of mean gray intensity for each horizontal line of images of the retina showing calbindin immunofluorescence. (**E, F**) Quantification of calbindin expression in the IPL sublaminae (**E**) and the number of calbindin+ cells per mm of retina (**F**) of control (*blue*) and HYA-treated (*red*) eyes. Data are represented as mean values of fluorescence in areas close to the optic nerve. ANOVA, Bonferroni's test, $^{**}P < 0.01$, n = 7 in each group. *Scale bar*: 40 µm (**A, B**), 20 µm (**C, D**).

to the ganglion cell layer and its dendrites stratify in the ON sublamina of the IPL (stratum S4). The other cell of the pair has its cell body in the amacrine cell layer with dendrites in the OFF sublamina of the IPL (stratum S2). Starburst amacrine cells interact with bipolar and other types of amacrine cells, receiving input from OFF or ON bipolar cells and likely also rod bipolar input via the AII amacrine cell pathway. They output to directionally-selective ganglion cells of the ON-type and the bistratified ON-OFF type.[65] Furthermore, ooDSGCs are the major and most extensively studied RGC subtype,[49,60–62] and can be distinguished from other RGCs by the expression of the neuropeptide CART. Four directionally-distinct ooDSGCs subtypes have been described based on their preferred direction: ventral, dorsal, nasal, or temporal motion on the retina.[49] These cells have their cell body placed in the ganglion cell layer and have bistratified dendrites that laminate in both OFF and ON sublaminae of the IPL. Within each sublamina, the dendrites contact with those of interneurons that provide excitatory or inhibitory input. The main source of excitatory input is provided by glutamatergic bipolar cells, and the inhibitory input is provided broadly by starburst amacrine cells. Thus starburst amacrine cells are a special type of neuron that support the release of two neurotransmitters: acetylcholine (excitatory), and GABA (inhibitory).[66,67] Whereas the cholinergic output may target various ganglion cell types[68] and lacks direction selectivity, it is accepted that the inhibitory output targets cells within the direction-selective circuitry, and starburst amacrine cells are essential elements in this circuitry because they are the source of directional signals in the retina.[62,66]

Our study provides evidence that intracameral HYA-injection induces a loss of ON/OFF starburst amacrine cells together with a loss of ooDSGCs and their plexuses.

However, there are conflicting reports regarding the differential susceptibility of the different retinal cells involved in the direction-selective circuit in glaucoma. Previous studies investigating the selective vulnerability of specific retinal cells using various glaucoma models have reported inconclusive and opposing results. Regarding starburst amacrine cells, some authors state that these cells were unaffected by glaucoma in the DBA/2J model.[29] Other studies using microbead-induced glaucoma models showed that only GABAergic amacrine cells were lost, and cholinergic cells remained unaffected.[31] Also, other authors reported a significant decline in both ON and OFF or only ON ChAT-positive starburst amacrine cells in episcleral vein cauterization[69] and hypertonic saline injection[70] models of glaucoma, respectively. Likely, these conflicting results can be attributed to the different procedures used to induce OHT and glaucoma conditions in the animal models. Comparatively, similar findings have been reported regarding RGC degeneration in different models of glaucoma. The hereditary DBA/2J model of glaucoma revealed that RGC degeneration was not cell-type specific but was different depending on the retinal region.[29] Nevertheless, different studies report a significant decline in different subtypes of ooDSGCs in microbead-injected,[43,50,71] optic nerve crush,[43,72] or laser-induced[73,74] glaucoma models. Thus most authors agree that ooDSGCs are highly vulnerable to glaucoma-like injury compared with other types of RGCs such as the non-image-forming intrinsically photosensitive RGCs. Additionally, to our knowledge, only one study using an ocular stroke model[75] has reported the degeneration of ON starburst amacrine cells together with ooDSGCs. Increased IOP correlates with a deficit in RGC axonal transport that precedes RGC damage, among other retinal disturbances, in the inner and outer nuclear layers, because of the impaired blood supply.[17,28] These harmful conditions generated by HYA-induced IOP that affect the RGCs, mainly ooDSGCs, may also contribute to the damage of other cell types in the retina, such as starburst amacrine cells.

Previous studies in patients with glaucoma have revealed an impairment in tasks processed early in the visual pathways and decreased motion perception sensitivity.[76–78] This alteration in motion perception was related to ganglion cell death in the retina, particularly, with the loss of magnocellular projecting parasol ganglion cells.[77,79] Likewise, some glaucoma animal models display permanent impairment of optokinetic response related to an impaired direction-selective circuit in the inner retina.[35,71,75,80]

Our work reveals that the abnormalities observed in glaucomatous patients related to motion perception may be not only due to the loss of magnocellular projecting ganglion cells, especially ooDSGCs, but also to the reduced number of starburst amacrine cells and a deteriorated ON/OFF plexus. Previous works demonstrated that psychophysical tests can be used as a diagnostic tool in patients suspected of having glaucomatous disease,[76–78] and this has been corroborated here in an animal glaucoma model.

Conclusions

Ocular hypertension triggered by intracameral serial HYA injection constitutes an easy and reproducible experimental model of glaucoma in rats, characterized by a subacute increase in IOP. In this model, the increased IOP triggered a significant loss of synaptic connectivity at the OPL and IPL. The loss of connections at the IPL was associated with the degeneration of RGCs but also amacrine cells. The degeneration of these specific cell types in glaucoma animal models might provide a feasible explanation for the visual deficiencies reported in patients with glaucoma diseases. In particular, the retinal direction-selective circuit is selectively vulnerable to IOP increase in our animal model, with a notable loss of ON/OFF starburst amacrine cells and ON-OFF direction-selective ganglion cells. Thus psychophysical tests could be a useful tool for the early diagnosis of glaucoma.

Acknowledgments

Supported by the Spanish Ministry of Science and Innovation (MICINN-FEDER PID2019-106230RB-I00), 2), Institute of Health Carlos III (General Subdirection of Networks and Cooperative Research Centers RETICs OFTARED 2012-2021) co-financed by the European Regional Development fund (RD16/0008/0016 [Alicante] and RD16/0008/0022 [Valencia]), Asociación Retina Asturias (ASOCIACIONRETINA1-20I), Generalitat Valenciana (IDIFEDER/2017/064), and the Research funds from both Department of Surgery (Ophthalmology Unit) and Cellular-Molecular Ophthalmobiology Group of the University of Valencia (Spain).

Disclosure: **A. Noailles**, None; **O. Kutsyr**, None; **A. Mayordomo-Febrer**, None; **P. Lax**, None; **M. López-Murcia**, None; **S.M. Sanz-González**, None; **M.D. Pinazo-Durán**, None; **N. Cuenca**, None

References

1. Calkins DJ. Critical pathogenic events underlying progression of neurodegeneration in glaucoma. *Progr Retinal Eye Res*. 2012;31:702–719.
2. Tanna AP. The challenge of detecting glaucoma progression. *Ophthalmology*. 2017;124(12):S49–S50.
3. Nickells RW. From ocular hypertension to ganglion cell death: A theoretical sequence of events leading to glaucoma. *Can J Ophthalmol*. 2007;42:278–287.
4. Williams AM, Huang W, Muir KW, Stinnett SS, Stone JS, Rosdahl JA. Identifying risk factors for blindness from primary open-angle glaucoma by race: a case-control study. *Clin Ophthalmol*. 2018;12:377–383.
5. Qu J, Wang D, Grosskreutz CL. Mechanisms of retinal ganglion cell injury and defense in glaucoma. *Exp Eye Res*. 2010;91:48–53.
6. Weinreb RN, Leung CKS, Crowston JG, et al. Primary open-angle glaucoma. *Nature Reviews Disease Primers*. 2016;2:1–9.
7. Pinazo-Durán MD, Muñoz-Negrete FJ, Sanz-Gonzalez SM, et al. The role of neuroinflammation in the pathogenesis of glaucoma neurodegeneration. *Progr Brain Res*. 2020;256:99–124.
8. Harada C, Kimura A, Guo X, Namekata K, Harada T. Recent advances in genetically modified animal models of glaucoma and their roles in drug repositioning. *Br J Ophthalmol*. 2019;103:161–166.
9. Biswas S, Wan KH. Review of rodent hypertensive glaucoma models. *Acta Ophthalmol*. 2019;97(3):e331–e340.
10. Albert-Fort M, Hombrebueno JR, Pons-Vazquez S, Sanz-Gonzalez S, Diaz-Llopis M, Pinazo-Durán MD. Retinal neurodegenerative changes in the adult insulin receptor substrate-2 deficient mouse. *Exp Eye Res*. 2014;124:1–10.
11. Chen H, Zhao Y, Liu M, et al. Progressive degeneration of retinal and superior collicular functions in mice with sustained ocular hypertension. *Invest Ophthalmol Vis Sci*. 2015;56:1971–1984.

12. Mayordomo-Febrer A, López-Murcia M, Morales-Tatay JM, Monleón-Salvado D, Pinazo-Durán MD. Metabolomics of the aqueous humor in the rat glaucoma model induced by a series of intracamerular sodium hyaluronate injection. *Exp Eye Res*. 2015;131:84–92.
13. Fortune B, Reynaud J, Hardin C, Wang L, Sigal IA, Burgoyne CF. Experimental glaucoma causes optic nerve head neural rim tissue compression: a potentially important mechanism of axon injury. *Invest Ophthalmol Vis Sci*. 2016;57:4403–4411.
14. Quigley HA. Use of animal models and techniques in glaucoma research: introduction. *Methods Mol Biol*. 2018;1695:1–10.
15. Vroemen PAMM, Gorgels TGMF, Webers CAB, De Boer J. Modeling the mechanical parameters of glaucoma. *Tissue Eng Part B Rev*. 2019;25:412–428.
16. Lambert WS, Carlson BJ, Ghose P, Vest VD, Yao V, Calkins DJ. Towards A Microbead Occlusion Model of Glaucoma for a Non-Human Primate. *Sci Rep*. 2019;9:1–15.
17. Cuenca N, Pinilla I, Fernández-Sánchez L, et al. Changes in the inner and outer retinal layers after acute increase of the intraocular pressure in adult albino Swiss mice. *Exp Eye Res*. 2010;91:273–285.
18. Morrison JC, Johnson EC, Cepurna WO. Hypertonic saline injection model of experimental glaucoma in rats. *Methods Mol Biol*. 2018;1695:11–21.
19. Moreno MC, Aldana Marcos HJ, Croxatto JO, et al. A new experimental model of glaucoma in rats through intracameral injections of hyaluronic acid. *Exp Eye Res*. 2005;81:71–80.
20. Cameron EG, Xia X, Galvao J, Ashouri M, Kapiloff MS, Goldberg JL. Optic nerve crush in mice to study retinal ganglion cell survival and regeneration. *Bio-protocols*. 2020;10(6).
21. Fernandes KA, Harder JM, Williams PA, et al. Using genetic mouse models to gain insight into glaucoma: Past results and future possibilities. *Exp Eye Res*. 2015;141:42–56.
22. Fernández-Sánchez LL, De Sevilla Müller LP, Brecha NC, Cuenca N. Loss of outer retinal neurons and circuitry alterations in the DBA/2J mouse. *Invest Ophthalmol Vis Sci*. 2014;55:6059–6072.
23. Turner AJ, Vander Wall R, Gupta V, Klistorner A, Graham SL. DBA/2J mouse model for experimental glaucoma: pitfalls and problems. *Clin Exp Ophthalmol*. 2017;45:911–922.
24. Cifuentes-Canorea P, Ruiz-Medrano J, Gutierrez-Bonet R, et al. Analysis of inner and outer retinal layers using spectral domain optical coherence tomography automated segmentation software in ocular hypertensive and glaucoma patients. *PLoS ONE*. 2018;13(4):1–12.
25. Unterlauft JD, Rehak M, Böhm MRR, Rauscher FG. Analyzing the impact of glaucoma on the macular architecture using spectral-domain optical coherence tomography. *PLoS ONE*. 2018;13(12):1–14.
26. Chen Z, Zheng X, Shen H, Zeng Z, Liu Q, Li Z. Combination of enhanced depth imaging optical coherence tomography and fundus images for glaucoma screening. *J Med Syst*. 2019;43(6):163.
27. Mitsch C, Holzer S, Wassermann L, et al. Comparison of Spectralis and Cirrus spectral domain optical coherence tomography for the objective morphometric assessment of the neuroretinal rim width. *Graefes Arch Clin Exp Ophthalmol*. 2019;257:1265–1275.
28. Vidal-Sanz M, Salinas-Navarro M, Nadal-Nicolás FM, et al. Understanding glaucomatous damage: anatomical and functional data from ocular hypertensive rodent retinas. *Progr Retin Eye Res*. 2012;31:1–27.
29. Jakobs TC, Libby RT, Ben Y, John SWM, Masland RH. Retinal ganglion cell degeneration is topological but not cell type specific in DBA/2J mice. *J Cell Biol*. 2005;171:313–325.
30. Benozzi J, Nahum LP, Campanelli JL, Rosenstein RE. Effect of hyaluronic acid on intraocular pressure in rats. *Invest Ophthalmol Vis Sci*. 2002;43:2196–2200.
31. Akopian A, Kumar S, Ramakrishnan H, Viswanathan S, Bloomfield SA. Amacrine cells coupled to ganglion cells via gap junctions are highly vulnerable in glaucomatous mouse retinas. *J Comp Neurol*. 2019;527:159–173.
32. Sarossy M, Crowston J, Kumar D, Weymouth A, Wu Z. Prediction of glaucoma severity using parameters from the electroretinogram. *Sci Rep*. 2021;11:1–9.
33. Jung KI, Jeon S, Shin DY, Lee J, Park CK. Pattern electroretinograms in preperimetric and perimetric glaucoma. *Am J Ophthalmol*. 2020;215:118–126.
34. Senger C, Moreto R, Watanabe SES, Matos AG, Paula JS. Electrophysiology in glaucoma. *J Glaucoma*. 2020;29:147–153.
35. Grillo SL, Koulen P. Psychophysical testing in rodent models of glaucomatous optic neuropathy. *Exp Eye Res*. 2014;141:154–163.
36. Noailles A, Maneu V, Campello L, Lax P, Cuenca N. Systemic inflammation induced by lipopolysaccharide aggravates inherited retinal dystrophy. *Cell Death Dis*. 2018;9:350.
37. Cuenca N, Fernández-Sánchez L, Campello L, et al. Cellular responses following retinal injuries and therapeutic approaches for neurodegenerative diseases. *Progr Retin Eye Res*. 2014;43:17–75.
38. Ramón y Cajal S. La Rétine Des Vertébrés. *La Cellule*. 1893;9:119–259.
39. Roska B, Werblin F. Vertical interactions across ten parallel, stacked representations in the mammalian retina. *Nature*. 2001;410(6828):583–587.
40. Mojumder DK, Wensel TG, Frishman LJ. Subcellular compartmentalization of two calcium binding proteins, calretinin and calbindin-28 kDa, in ganglion and amacrine cells of the rat retina. *Mol Vis*. 2008;14:1600–1613.
41. Brandstätter JH, Greferath U, Euler T, Wässle H. Co-stratification of gabaa receptors with the directionally selective circuitry of the rat retina. *Vis Neurosci*. 1995;12:345–358.
42. De La Huerta I, Kim IJ, Voinescu PE, Sanes JR. Direction-selective retinal ganglion cells arise from molecularly specified multipotential progenitors. *Proc Natl Acad Sci USA*. 2012;109:17663–17668.
43. VanderWall KB, Lu B, Alfaro JS, et al. Differential susceptibility of retinal ganglion cell subtypes in acute and chronic models of injury and disease. *Sci Rep*. 2020;10:1–10.
44. Moreno MC, de Zavalía N, Sande P, et al. Effect of ocular hypertension on retinal GABAergic activity. *Neurochem Int*. 2008;52:675–682.
45. Belforte N, Moreno MC, Cymeryng C, Bordone M, Keller Sarmiento MI, Rosenstein RE. Effect of ocular hypertension on retinal nitridergic pathway activity. *Invest Ophthalmol Vis Sci*. 2007;48:2127–2133.
46. Shmulevich A, Beit-Yannai E. Differential modulation of MAPKs in relation to increased intraocular pressure in the aqueous humor of rat eye injected with hyaluronic acid. *Curr Eye Res*. 2009;34:466–475.
47. Emre E, Yüksel N, Duruksu G, et al. Neuroprotective effects of intravitreally transplanted adipose tissue and bone marrow-derived mesenchymal stem cells in an experimental ocular hypertension model. *Cytotherapy*. 2015;17(5):543–559.
48. Guo C, Qu X, Rangaswamy N, et al. A murine glaucoma model induced by rapid in vivo photopolymerization of hyaluronic acid glycidyl methacrylate. *PLoS ONE*. 2018;13(6):e0196529.
49. Kay JN, de la Huerta I, Kim IJ, et al. Retinal ganglion cells with distinct directional preferences differ in molecular

Investigative Ophthalmology & Visual Science

identity, structure, and central projections. *J Neurosci*. 2011;31:7753–7762.
50. Risner ML, Pasini S, Cooper ML, Lambert WS, Calkins DJ. Axogenic mechanism enhances retinal ganglion cell excitability during early progression in glaucoma. *Proc Natl Acad Sci USA*. 2018;115(10):E2393–E2402.
51. Vidal-Sanz M, Valiente-Soriano FJ, Ortín-Martínez A, et al. Retinal neurodegeneration in experimental glaucoma. *Prog Brain Res*. 2015;220:1–35.
52. Fuchs M, Scholz M, Sendelbeck A, et al. Rod photoreceptor ribbon synapses in DBA/2J mice show progressive age-related structural changes. *PLoS ONE*. 2012;7(9):1–10.
53. Mukherjee K, Yang X, Gerber SH, et al. Piccolo and bassoon maintain synaptic vesicle clustering without directly participating in vesicle exocytosis. *Proc Natl Acad Sci USA*. 2010;107:6504–6509.
54. Johnson JE, Perkins GA, Giddabasappa A, et al. Spatiotemporal regulation of ATP and Ca2+ dynamics in vertebrate rod and cone ribbon synapses. *Mol Vis*. 2007;13:887–919.
55. Medrano CJ, Fox DA. Oxygen consumption in the rat outer and inner retina: Light- and pharmacologically-induced inhibition. *Exp Eye Res*. 1995;61:273–284.
56. Park HYL, Kim JH, Park CK. Alterations of the synapse of the inner retinal layers after chronic intraocular pressure elevation in glaucoma animal model. *Mol Brain*. 2014;7(1):53.
57. Choi SS, Zawadzki RJ, Lim MC, et al. Evidence of outer retinal changes in glaucoma patients as revealed by ultrahigh-resolution in vivo retinal imaging. *Br J Ophthalmol*. 2011;95:131–141.
58. Lei Y, Garrahan N, Hermann B, et al. Quantification of retinal transneuronal degeneration in human glaucoma: A novel multiphoton-DAPI approach. *Invest Ophthalmol Vis Sci*. 2008;49:1940–1945.
59. Lei Y, Garrahan N, Hermann B, et al. Transretinal degeneration in ageing human retina: A multiphoton microscopy analysis. *Br J Ophthalmol*. 2011;95:727–730.
60. Rasmussen R, Yonehara K. Contributions of retinal direction selectivity to central visual processing. *Curr Biol*. 2020;30(15):R897–R903.
61. Hamilton NR, Scasny AJ, Kolodkin AL. Development of the vertebrate retinal direction-selective circuit. *Dev Biol*. 2021;477:273–283.
62. Wei W, Feller MB. Organization and development of direction-selective circuits in the retina. *Trends Neurosci*. 2011;34:638–645.
63. Masland RH, Mills JW. Autoradiographic identification of acetylcholine in the rabbit retina. *J Cell Biol*. 1979;83:159–178.
64. Cuenca N, Deng P, Linberg KA, Fisher SK, Kolb H. Choline acetyltransferase is expressed by non-starburst amacrine cells in the ground squirrel retina. *Brain Res*. 2003;964:21–30.
65. Famiglietti E V. Synaptic organization of complex ganglion cells in rabbit retina: Type and arrangement of inputs to directionally selective and local-edge-detector cells. *J Comp Neurol*. 2005;484:357–391.
66. Taylor WR, Smith RG. The role of starburst amacrine cells in visual signal processing. *Vis Neurosci*. 2012;29:73–81.
67. O'Malley DM, Masland RH. Co-release of acetylcholine and γ-aminobutyric acid by a retinal neuron. *Proc Natl Acad Sci USA*. 1989;86:3414–3418.
68. Vaney DI, Pow D V. The dendritic architecture of the cholinergic plexus in the rabbit retina: Selective labeling by glycine accumulation in the presence of sarcosine. *J Comp Neurol*. 2000;421:1–13.
69. Hernandez M, Rodriguez FD, Sharma SC, Vecino E. Immunohistochemical changes in rat retinas at various time periods of elevated intraocular pressure. *Mol Vis*. 2009;15:2696–2709.
70. Cooley-Themm C, Ameel Q, Linn D, Linn C. Loss of displaced starburst amacrine cells in a rat glaucoma model. *J Ophthalmic Res Ocul Care*. 2017;1(1):.
71. Della Santina L, Inman DM, Lupien CB, Horner PJ, Wong ROL. Differential progression of structural and functional alterations in distinct retinal ganglion cell types in a mouse model of glaucoma. *J Neurosci*. 2013;33:17444–17457.
72. Daniel S, Clark A, McDowell C. Subtype-specific response of retinal ganglion cells to optic nerve crush. *Cell Death Discov*. 2018;4:1–16.
73. Feng L, Zhao Y, Yoshida M, et al. Sustained ocular hypertension induces dendritic degeneration of mouse retinal ganglion cells that depends on cell type and location. *Invest Ophthalmol Vis Sci*. 2013;54:1106–1117.
74. Ou Y, Jo RE, Ullian EM, Wong ROL, Della Santina L. Selective vulnerability of specific retinal ganglion cell types and synapses after transient ocular hypertension. *J Neurosci*. 2016;36:9240–9252.
75. Joly S, Guzik-Kornacka A, Schwab ME, Pernet V. New mouse retinal stroke model reveals direction-selective circuit damage linked to permanent optokinetic response loss. *Invest Ophthalmol Vis Sci*. 2014;55:4476–4489.
76. McKendrick AM, Badcock DR, Morgan WH. The detection of both global motion and global form is disrupted in glaucoma. *Invest Ophthalmol Vis Sci*. 2005;46:3693–3701.
77. Karwatsky P, Bertone A, Overbury O, Faubert J. Defining the nature of motion perception deficits in glaucoma using simple and complex motion stimuli. *Optom Vis Sci*. 2006;83:466–472.
78. Shabana N, Cornilleau Pérès V, Carkeet A, Chew PTK. Motion perception in glaucoma patients: a review. *Surv Ophthalmol*. 2003;48:92–106.
79. Anderson RS, O'Brien C. Psychophysical evidence for a selective loss of M ganglion cells in glaucoma. *Vis Res*. 1997;37:1079–1083.
80. Yoshida K, Watanabe D, Ishikane H, Tachibana M, Pastan I, Nakanishi S. A key role of starburst amacrine cells in originating retinal directional selectivity and optokinetic eye movement. *Neuron*. 2001;30:771–780.

Investigative Ophthalmology & Visual Science